The Astrophysical Journal Letters, 815:L23 (8pp), 2015 December 20 doi:10.1088/2041-8205/815/2/L23

VERY HIGH ENERGY γ-RAYS FROM THE UNIVERSE'S MIDDLE AGE: DETECTION OF THE $z = 0.940$ BLAZAR PKS 1441+25 WITH MAGIC

M. L. Ahnen[1], S. Ansoldi[2], L. A. Antonelli[3], P. Antoranz[4], A. Babic[5], B. Banerjee[6], P. Bangale[7], U. Barres de Almeida[7,74], J. A. Barrio[8], W. Bednarek[9], E. Bernardini[10,11], B. Biasuzzi[2], A. Biland[1], O. Blanch[12], S. Bonnefoy[8], G. Bonnoli[3], F. Borracci[7], T. Bretz[13,75], E. Carmona[14], A. Carosi[3], A. Chatterjee[6], R. Clavero[15,16], P. Colin[7], E. Colombo[15,16], J. L. Contreras[8], J. Cortina[12], S. Covino[3], P. Da Vela[4], F. Dazzi[7], A. De Angelis[17], B. De Lotto[2], E. de Oña Wilhelmi[18], C. Delgado Mendez[14], F. Di Pierro[3], D. Dominis Prester[5], D. Dorner[13], M. Doro[7,19], S. Einecke[20], D. Eisenacher Glawion[13], D. Elsaesser[13], A. Fernández-Barral[12], D. Fidalgo[8], M. V. Fonseca[8], L. Font[21], K. Frantzen[20], C. Fruck[7], D. Galindo[22], R. J. García López[15,16], M. Garczarczyk[10], D. Garrido Terrats[21], M. Gaug[21], P. Giammaria[3], N. Godinović[5], A. González Muñoz[12], D. Guberman[12], A. Hahn[7], Y. Hanabata[23], M. Hayashida[23], J. Herrera[15,16], J. Hose[7], D. Hrupec[5], G. Hughes[1], W. Idec[9], K. Kodani[23], Y. Konno[23], H. Kubo[23], J. Kushida[23], A. La Barbera[3], D. Lelas[5], E. Lindfors[24], S. Lombardi[3], M. López[8], R. López-Coto[12], A. López-Oramas[12,76], E. Lorenz[7], P. Majumdar[6], M. Makariev[25], K. Mallot[10], G. Maneva[25], M. Manganaro[15,16], K. Mannheim[13], L. Maraschi[3], B. Marcote[22], M. Mariotti[17], M. Martínez[12], D. Mazin[7,23], U. Menzel[7], J. M. Miranda[4], R. Mirzoyan[7], A. Moralejo[12], E. Moretti[7], D. Nakajima[23], V. Neustroev[24], A. Niedzwiecki[9], M. Nievas Rosillo[8], K. Nilsson[24,77], K. Nishijima[23], K. Noda[7], R. Orito[23], A. Overkemping[20], S. Paiano[17], J. Palacio[12], M. Palatiello[2], D. Paneque[7], R. Paoletti[4], J. M. Paredes[22], X. Paredes-Fortuny[22], M. Persic[2,78], J. Poutanen[24], P. G. Prada Moroni[26], E. Prandini[1,79], I. Puljak[5], W. Rhode[20], M. Ribó[22], J. Rico[12], J. Rodriguez Garcia[7], T. Saito[23], K. Satalecka[8], C. Schultz[17], T. Schweizer[7], S. N. Shore[26], A. Sillanpää[24], J. Sitarek[9], I. Snidaric[5], D. Sobczynska[9], A. Stamerra[3], T. Steinbring[13], M. Strzys[7], L. Takalo[24], H. Takami[23], F. Tavecchio[3], P. Temnikov[25], T. Terzić[5], D. Tescaro[15,16], M. Teshima[7,23], J. Thaele[20], D. F. Torres[27], T. Toyama[7], A. Treves[28], V. Verguilov[25], I. Vovk[7], J. E. Ward[12], M. Will[15,16], M. H. Wu[18], R. Zanin[22] (MAGIC Collaboration), M. Ajello[29], L. Baldini[30,31], G. Barbiellini[32,33], D. Bastieri[19,34], J. Becerra González[15,16,35,36], R. Bellazzini[37], E. Bissaldi[38], R. D. Blandford[31], R. Bonino[39,40], J. Bregeon[41], P. Bruel[42], S. Buson[19,34], G. A. Caliandro[31,43], R. A. Cameron[31], M. Caragiulo[38], P. A. Caraveo[44], E. Cavazzuti[45], J. Chiang[31], G. Chiaro[34], S. Ciprini[45,46,47], F. D'Ammando[48,49], F. de Palma[38,50], R. Desiante[39,51], L. Di Venere[52], A. Domínguez[29], P. Fusco[38,52], F. Gargano[38], D. Gasparrini[45,46,47], N. Giglietto[38,52], F. Giordano[38,52], M. Giroletti[48], I. A. Grenier[53], S. Guiriec[35,80], E. Hays[35], J. W. Hewitt[54], T. Jogler[31], M. Kuss[37], S. Larsson[55,56], J. Li[18], L. Li[55,56], F. Longo[32,33], F. Loparco[38,52], M. N. Lovellette[57], P. Lubrano[46,58], S. Maldera[39], M. Mayer[10], M. N. Mazziotta[38], J. E. McEnery[35,36], N. Mirabal[35,80], T. Mizuno[59], M. E. Monzani[31], A. Morselli[60], I. V. Moskalenko[31], E. Nuss[41], R. Ojha[35,61,62], T. Ohsugi[59], N. Omodei[31], E. Orlando[31], J. S. Perkins[35], M. Pesce-Rollins[31,37], F. Piron[41], G. Pivato[37], T. A. Porter[31], S. Raino[38,52], R. Rando[19,34], M. Razzano[37,81], A. Reimer[31,63], O. Reimer[31,63], C. Sgro[37], E. J. Siskind[64], F. Spada[37], G. Spandre[37], P. Spinelli[38,52], H. Tajima[31,65], H. Takahashi[66], J. B. Thayer[31], D. J. Thompson[35], E. Troja[35,37], K. S. Wood[57] (Fermi-LAT Collaboration), M. Balokovic[67], A. Berdyugin[68], A. Carraminana[69], L. Carrasco[69], V. Chavushyan[69], V. Fallah Ramazani[68], M. Feige[70], S. Haarto[71], P. Haeusner[70], T. Hovatta[67,71], J. Kania[70], J. Klamt[70], A. Lähteenmäki[71,72], J. Leon-Tavares[69], C. Lorey[70], L. Pacciani[73], A. Porras[69], E. Recillas[69], R. Reinthal[68], M. Tornikoski[71], D. Wolfert[70], and N. Zottmann[70]

[1] ETH Zurich, CH-8093 Zurich, Switzerland
[2] Università di Udine, and INFN Trieste, I-33100 Udine, Italy
[3] INAF National Institute for Astrophysics, I-00136 Rome, Italy; fabrizio.tavecchio@brera.inaf.it
[4] Università di Siena, and INFN Pisa, I-53100 Siena, Italy
[5] Croatian MAGIC Consortium, Rudjer Boskovic Institute, University of Rijeka, University of Split and University of Zagreb, Croatia
[6] Saha Institute of Nuclear Physics, 1\AF Bidhannagar, Salt Lake, Sector-1, Kolkata 700064, India
[7] Max-Planck-Institut für Physik, D-80805 München, Germany
[8] Universidad Complutense, E-28040 Madrid, Spain; miguelnievas@ucm.es
[9] University of Łódź, PL-90236 Lodz, Poland
[10] Deutsches Elektronen-Synchrotron (DESY), D-15738 Zeuthen, Germany
[11] Humboldt University of Berlin, Istitut für Physik Newtonstr. 15, D-12489 Berlin Germany
[12] IFAE, Campus UAB, E-08193 Bellaterra, Spain
[13] Universität Würzburg, D-97074 Würzburg, Germany
[14] Centro de Investigaciones Energéticas, Medioambientales y Tecnológicas, E-28040 Madrid, Spain
[15] Inst. de Astrofísica de Canarias, E-38200 La Laguna, Tenerife, Spain; manganaro@iac.es
[16] Universidad de La Laguna, Dpto. Astrofísica, E-38206 La Laguna, Tenerife, Spain
[17] Università di Padova and INFN, I-35131 Padova, Italy
[18] Institute for Space Sciences (CSIC\IEEC), E-08193 Barcelona, Spain
[19] Istituto Nazionale di Fisica Nucleare, Sezione di Padova, I-35131 Padova, Italy
[20] Technische Universität Dortmund, D-44221 Dortmund, Germany
[21] Unitat de Física de les Radiacions, Departament de Física, and CERES-IEEC, Universitat Autònoma de Barcelona, E-08193 Bellaterra, Spain
[22] Universitat de Barcelona, ICC, IEEC-UB, E-08028 Barcelona, Spain
[23] Japanese MAGIC Consortium, ICRR, The University of Tokyo, Department of Physics and Hakubi Center, Kyoto University, Tokai University, The University of Tokushima, KEK, Japan
[24] Finnish MAGIC Consortium, Tuorla Observatory, University of Turku and Department of Physics, University of Oulu, Finland

[25] Inst. for Nucl. Research and Nucl. Energy, BG-1784 Sofia, Bulgaria
[26] Università di Pisa, and INFN Pisa, I-56126 Pisa, Italy
[27] ICREA and Institute for Space Sciences (CSIC\IEEC), E-08193 Barcelona, Spain
[28] Università dell'Insubria and INFN Milano Bicocca, Como, I-22100 Como, Italy
[29] Department of Physics and Astronomy, Clemson University, Kinard Lab of Physics, Clemson, SC 29634-0978, USA
[30] Università di Pisa and Istituto Nazionale di Fisica Nucleare, Sezione di Pisa I-56127 Pisa, Italy
[31] W. W. Hansen Experimental Physics Laboratory, Kavli Institute for Particle Astrophysics and Cosmology, Department of Physics and SLAC National Accelerator Laboratory, Stanford University, Stanford, CA 94305, USA
[32] Istituto Nazionale di Fisica Nucleare, Sezione di Trieste, I-34127 Trieste, Italy
[33] Dipartimento di Fisica, Università di Trieste, I-34127 Trieste, Italy
[34] Dipartimento di Fisica e Astronomia "G. Galilei," Università di Padova, I-35131 Padova, Italy
[35] NASA Goddard Space Flight Center, Greenbelt, MD 20771, USA; josefa.becerra@nasa.gov
[36] Department of Physics and Department of Astronomy, University of Maryland, College Park, MD 20742, USA
[37] Istituto Nazionale di Fisica Nucleare, Sezione di Pisa, I-56127 Pisa, Italy
[38] Istituto Nazionale di Fisica Nucleare, Sezione di Bari, I-70126 Bari, Italy
[39] Istituto Nazionale di Fisica Nucleare, Sezione di Torino, I-10125 Torino, Italy
[40] Dipartimento di Fisica Generale "Amadeo Avogadro," Università degli Studi di Torino, I-10125 Torino, Italy
[41] Laboratoire Univers et Particules de Montpellier, Université Montpellier, CNRS/IN2P3, Montpellier, France
[42] Laboratoire Leprince-Ringuet, École polytechnique, CNRS/IN2P3, Palaiseau, France
[43] Consorzio Interuniversitario per la Fisica Spaziale (CIFS), I-10133 Torino, Italy
[44] INAF-Istituto di Astrofisica Spaziale e Fisica Cosmica, I-20133 Milano, Italy
[45] Agenzia Spaziale Italiana (ASI) Science Data Center, I-00133 Roma, Italy
[46] Istituto Nazionale di Fisica Nucleare, Sezione di Perugia, I-06123 Perugia, Italy
[47] INAF Osservatorio Astronomico di Roma, I-00040 Monte Porzio Catone (Roma), Italy
[48] INAF Istituto di Radioastronomia, I-40129 Bologna, Italy
[49] Dipartimento di Astronomia, Università di Bologna, I-40127 Bologna, Italy
[50] Università Telematica Pegaso, Piazza Trieste e Trento, 48, I-80132 Napoli, Italy
[51] Università di Udine, I-33100 Udine, Italy
[52] Dipartimento di Fisica "M. Merlin" dell'Università e del Politecnico di Bari, I-70126 Bari, Italy
[53] Laboratoire AIM, CEA-IRFU/CNRS/Université Paris Diderot, Service d'Astrophysique, CEA Saclay, F-91191 Gif sur Yvette, France
[54] University of North Florida, Department of Physics, 1 UNF Drive, Jacksonville, FL 32224 , USA
[55] Department of Physics, KTH Royal Institute of Technology, AlbaNova, SE-106 91 Stockholm, Sweden
[56] The Oskar Klein Centre for Cosmoparticle Physics, AlbaNova, SE-106 91 Stockholm, Sweden
[57] Space Science Division, Naval Research Laboratory, Washington, DC 20375-5352, USA
[58] Dipartimento di Fisica, Università degli Studi di Perugia, I-06123 Perugia, Italy
[59] Hiroshima Astrophysical Science Center, Hiroshima University, Higashi-Hiroshima, Hiroshima 739-8526, Japan
[60] Istituto Nazionale di Fisica Nucleare, Sezione di Roma "Tor Vergata," I-00133 Roma, Italy
[61] Catholic University of America, Washington, DC 20064, USA
[62] University of Maryland, Baltimore County, Baltimore, MD 21250, USA
[63] Institut für Astro- und Teilchenphysik and Institut für Theoretische Physik, Leopold-Franzens-Universität Innsbruck, A-6020 Innsbruck, Austria
[64] NYCB Real-Time Computing Inc., Lattingtown, NY 11560-1025, USA
[65] Solar-Terrestrial Environment Laboratory, Nagoya University, Nagoya 464-8601, Japan
[66] Department of Physical Sciences, Hiroshima University, Higashi-Hiroshima, Hiroshima 739-8526, Japan
[67] Cahill Center for Astrophysics, 1216 East California Boulevard, California Institute of Technology, Pasadena, CA 91125, USA
[68] Tuorla Observatory, Department of Physics and Astronomy, University of Turku, Finland
[69] Instituto Nacional de Astrofísica Óptica y Electrónica (INAOE), Apartado Postal 51 y 216, 72000 Puebla, México
[70] Naturwissenschaftliches Labor für Schüler, Friedrich-Koenig-Gymnasium, Würzburg, Germany
[71] Aalto University Metsähovi Radio Observatory, Metsähovintie 114, FI-02540 Kylmälä, Finland
[72] Aalto University Department of Radio Science and Engineering, P.O. BOX 13000, FI-00076 AALTO, Finland
[73] INAF-Istituto di Astrofisica e Planetologia Spaziale, Via Fosso del Cavaliere 100, I-00133 Rome, Italy
Received 2015 August 11; accepted 2015 November 22; published 2015 December 15

ABSTRACT

The flat-spectrum radio quasar PKS 1441+25 at a redshift of $z = 0.940$ is detected between 40 and 250 GeV with a significance of 25.5σ using the MAGIC telescopes. Together with the gravitationally lensed blazar QSO B0218 +357 ($z = 0.944$), PKS 1441+25 is the most distant very high energy (VHE) blazar detected to date. The observations were triggered by an outburst in 2015 April seen at GeV energies with the Large Area Telescope on board *Fermi*. Multi-wavelength observations suggest a subdivision of the high state into two distinct flux states. In the band covered by MAGIC, the variability timescale is estimated to be 6.4 ± 1.9 days. Modeling the broadband spectral energy distribution with an external Compton model, the location of the emitting region is understood as originating in the jet outside the broad-line region (BLR) during the period of high activity, while being partially within the BLR during the period of low (typical) activity. The observed VHE spectrum during the highest activity

[74] Now at Centro Brasileiro de Pesquisas Físicas (CBPF/MCTI), R. Dr. Xavier Sigaud, 150, Urca, Rio de Janeiro, RJ 22290-180, Brazil.
[75] Now at Ecole polytechnique fédérale de Lausanne (EPFL), Lausanne, Switzerland.
[76] Now at Laboratoire AIM, Service d'Astrophysique, DSM/IRFU, CEA/Saclay FR-91191 Gif-sur-Yvette Cedex, France.
[77] Now at Finnish Centre for Astronomy with ESO (FINCA), Turku, Finland.
[78] Also at INAF-Trieste.
[79] Also at ISDC—Science Data Center for Astrophysics, 1290, Versoix (Geneva).
[80] NASA Postdoctoral Program Fellow, USA.
[81] Funded by contract FIRB-2012-RBFR12PM1F from the Italian Ministry of Education, University and Research (MIUR).

is used to probe the extragalactic background light at an unprecedented distance scale for ground-based gamma-ray astronomy.

Key words: cosmic background radiation – galaxies: active – galaxies: jets – gamma rays: galaxies – quasars: individual (PKS 1441+25)

1. INTRODUCTION

PKS 1441+25 is a known high-energy (HE; 0.1 GeV $< E <$ 100 GeV) γ-ray flat spectrum radio quasar (FSRQ) (Abdo et al. 2010a; Nolan et al. 2012; Ackermann et al. 2013) located at $z = 0.9397 \pm 0.0003_{\rm stat}$[82]. In 2015 January it became active from γ-rays to the near-infrared (Carrasco et al. 2015; Ojha 2015; Pacciani 2015; Pursimo & Ojha 2015). In April, the detection of the source with a hard spectral index with the *Fermi Gamma-ray Space* Large Area Telescope (LAT) together with increased multi-wavelength (MWL) emission triggered the MAGIC observations. They resulted in the first detection of this source at very high energy (VHE, $E >$ 100 GeV; Mirzoyan 2015), later followed up by VERITAS (Mukherjee 2015). This detection makes PKS1441+25 the[83] 5th FSRQ with a firm classification detected at VHE, and the most distant known VHE source, along with QSO B0218+357 ($z = 0.944 \pm 0.002$; Sitarek et al. 2015).

In this letter, the MWL observations are discussed in the context of an external Compton model for four different states of activity, dubbed periods A (MJD 57125.0–57130.0), B (57130.0–57135.5), C (57135.5–57139.5) and D (57149.0–57156.0). Upper limits on the extragalactic background light (EBL) are obtained in the VHE band.

2. OBSERVATIONS AND ANALYSIS

2.1. VHE γ-Ray Observations

MAGIC is a stereoscopic system consisting of two 17 m diameter Imaging Atmospheric Cherenkov Telescopes located at the Observatorio del Roque de los Muchachos, on the Canary Island of La Palma. The current sensitivity for low-zenith observations ($zd < 30°$) above 220 GeV is $0.66 \pm 0.03\%$ of the Crab Nebula's flux in 50 hr (Aleksić et al. 2015).

The MAGIC telescopes monitored PKS 1441+25 from 2015 April 18 to 27 (MJD 57130–57139, for a total of 29.9 hr) and May 8–9 (MJD 57150–57151, for 1.8 hr), the observational gap being due to the full-moon break. The observations were performed in wobble mode with a $0.^{\circ}4$ offset and four symmetric positions with respect to the camera center (Fomin et al. 1994). The data were collected in the zenith angle range of $3° < zd < 38°$.

The analysis of the data is performed using the standard MAGIC analysis framework *MARS* (Zanin et al. 2013; Aleksić et al. 2015) and Monte Carlo (MC) simulations matching the night-sky background levels.

PKS 1441+25 is detected with a significance of 25.5σ (γ-ray-like excess $N_{\rm ex} = 4010 \pm 160$) during periods B+C. No significant emission was found in period D.

The differential VHE spectrum is measured from 40 to 250 GeV and 50–160 GeV in periods B and C respectively. A power-law (PWL) can describe both observed and EBL-corrected spectra using the model of Domínguez et al. (2011):

$$\frac{dF}{dE} = f_0 \left(\frac{E}{100\ \text{GeV}} \right)^{-\Gamma}, \quad (1)$$

where the normalization constant f_0, the spectral index Γ and the goodness of the fit (χ^2/ndf and p-value) are:

1. Period B:
   (i) Observed: $f_0 = (1.14 \pm 0.06_{\rm stat} \pm 0.20_{\rm sys}) \times 10^{-9}$ cm^{-2} s^{-1} TeV^{-1} and $\Gamma = 4.62 \pm 0.11_{\rm stat} \pm 0.18_{\rm sys}$ ($\chi^2/ndf = 22.9/6$, $P = 8.4 \times 10^{-4}$)
   (ii) EBL-corrected: $f_0 = (2.7 \pm 0.1_{\rm stat} \pm 0.5_{\rm sys}) \times 10^{-9}$ cm^{-2} s^{-1} TeV^{-1} and $\Gamma = 3.18 \pm 0.15_{\rm stat} \pm 0.18_{\rm sys}$ ($\chi^2/ndf = 5.6/6$, $P = 0.47$)
2. Period C:
   (i) Observed: $f_0 = (0.82 \pm 0.09_{\rm stat} \pm 0.13_{\rm sys}) \times 10^{-9}$ cm^{-2} s^{-1} TeV^{-1} and $\Gamma = 3.7 \pm 0.4_{\rm stat} \pm 0.2_{\rm sys}$ ($\chi^2/ndf = 2.7/3$, $P = 0.44$)
   (ii) EBL-corrected: $f_0 = (1.7 \pm 0.2_{\rm stat} \pm 0.3_{\rm sys}) \times 10^{-9}$ cm^{-2} s^{-1} TeV^{-1} and $\Gamma = 2.5 \pm 0.4_{\rm stat} \pm 0.2_{\rm sys}$ ($\chi^2/ndf = 4.3/3$, $P = 0.23$).

From a likelihood ratio test (LRT), a model with intrinsic curvature such as a log-parabola (LP) is preferred at 4.2 σ during period B. It is defined as:

$$\frac{dF}{dE} = f_0 \left(\frac{E}{100\ \text{GeV}} \right)^{-\Gamma_{\rm LP} - b \log_{10} \frac{E}{100\ \text{GeV}}}, \quad (2)$$

where $f_0 = (1.39 \pm 0.09_{\rm stat} \pm 0.24_{\rm sys}) \times 10^{-9}$ cm^{-2} s^{-1}TeV^{-1}, $\Gamma_{\rm LP} = 4.69 \pm 0.16_{\rm stat}$ and $b = 3.2 \pm 1.0_{\rm stat}$ ($\chi^2/ndf = 5.2/5$, $P = 0.39$). A full description of the MAGIC systematic uncertainties can be found in Aleksić et al. (2015) and references therein.

2.2. HE γ-Ray Observations

In nominal survey mode the LAT monitors the entire γ-ray sky every 3 hr in the energy range from 20 MeV to at least 300 GeV (Atwood et al. 2009). We select Pass 8 SOURCE class events collected from 2015 April 8 to May 23 (MJD 57120–57165) between 100 MeV to 500 GeV and within a 10° Region of Interest (ROI) centered at the location of PKS 1441+25. In order to reduce contamination from the Earth Limb, a zenith angle cut of <90° is applied. The analysis is performed with the ScienceTools software package version v10r0p5 using the `P8R2_SOURCE_V6`[84] instrument response functions and the `gll_iem_v06` and `iso_P8R2_SOURCE_V6_v06` models[85] for the Galactic and isotropic diffuse emission, respectively.

The likelihood fit is performed using `gtlike`, including all 3FGL sources (Acero et al. 2015) within 20° from PKS 1441+25. The spectral indices and fluxes are left free for sources

[82] From SDSS: http://skyserver.sdss.org/dr10/en/get/SpecById.ashx?id=6780257851631206400; see also Shaw et al. (2012).
[83] http://tevcat.uchicago.edu
[84] http://fermi.gsfc.nasa.gov/ssc/data/analysis/documentation/Cicerone/Cicerone_LAT_IRFs/IRF_overview.html
[85] http://fermi.gsfc.nasa.gov/ssc/data/access/lat/BackgroundModels.html

within 10°, while sources from 10° to 20° have their parameters fixed to the catalog value. Both the flux and the spectral index of PKS 1441+25 are left free for the light curve calculation, while the parameters for the rest of the sources in the ROI are fixed except the diffuse components. Five photons of energies 10–50 GeV were detected with a probability of association with PKS 1441+25 larger than 99.6%, calculated with `gtsrcprob`. The spectrum of PKS 1441+25 is well fit by a PWL (as in the 3FGL catalog) and no significant curvature was found. During the flare (period B+C), the spectral index is $\Gamma = 1.75 \pm 0.06$, harder than the 3FGL value $\Gamma_{3FGL} = 2.13 \pm 0.07$.

2.3. Hard X-Ray Observations

NuSTAR (*Nuclear Spectroscopic Telescope Array*; Harrison et al. 2013) is a hard X-ray telescope operating in the energy range between 3 and 79 keV. PKS 1441+25 was observed with *NuSTAR* on 2015 April 25–26 (MJD 57137.1113) for a total (on-source) exposure of 40 ks. The data are processed using the standard `nupipeline` script (version 1.4.1) available in the NuSTARDAS software package (Perri et al. 2014). The source spectrum extends up to ≃25 keV, and can be described by a PWL with spectral index $\Gamma = 2.30 \pm 0.08$ ($\chi^2/ndf = 10.4/7$). No significant variability is detected during the observation.

2.4. X-Ray and Optical–UV Observations

A *Swift* (Gehrels 2004) target of opportunity started on 2015 April 15. *Swift*-XRT (Burrows et al. 2005) observed the source in photon-counting mode. Standard filtering and analysis of the data were employed. The source exhibited a soft X-ray photon index (from 1.94 ± 0.16 to 2.55 ± 0.24) and is described by an absorbed PWL model, with the Galactic absorption fixed to $N_H = 3.2 \times 10^{20}\,\mathrm{cm}^{-2}$ (Kalberla et al. 2005) during April–May 2015. For comparison, the observations on 2010 June 12 (MJD 55359) can be fit with a PWL with spectral index 1.2 ± 0.3.

The *Swift*-UVOT (Roming et al. 2005) flux in several bands was estimated using aperture photometry. De-reddening is performed using $E(B-V) = 0.033$ (Schlafly & Finkbeiner 2011) and $A_V/E(B-V) = 3.1$ (Schultz & Wiemer 1975).

2.5. Optical Observations

Optical R-band observations started on MJD 57130 and were performed using the 35 cm Celestron telescope attached to the KVA[86] 60 cm telescope (La Palma, Canary Islands, Spain) and the 50 cm Hans-Haffner-Telescope (Hettstadt, Würzburg, Germany).[87] The data are analyzed using differential photometry and corrected for Galactic extinction (Schlafly & Finkbeiner 2011). The host galaxy contribution is negligible compared to the flux of the source during these observations. The optical emission shows a high degree of polarization, reaching a maximum of 37.7% on MJD 57132 (Smith & Tutar Ozdarcan 2015).

[86] http://users.utu.fi/kani/1m

[87] http://schuelerlabor-wuerzburg.de/?p = Sternwarte

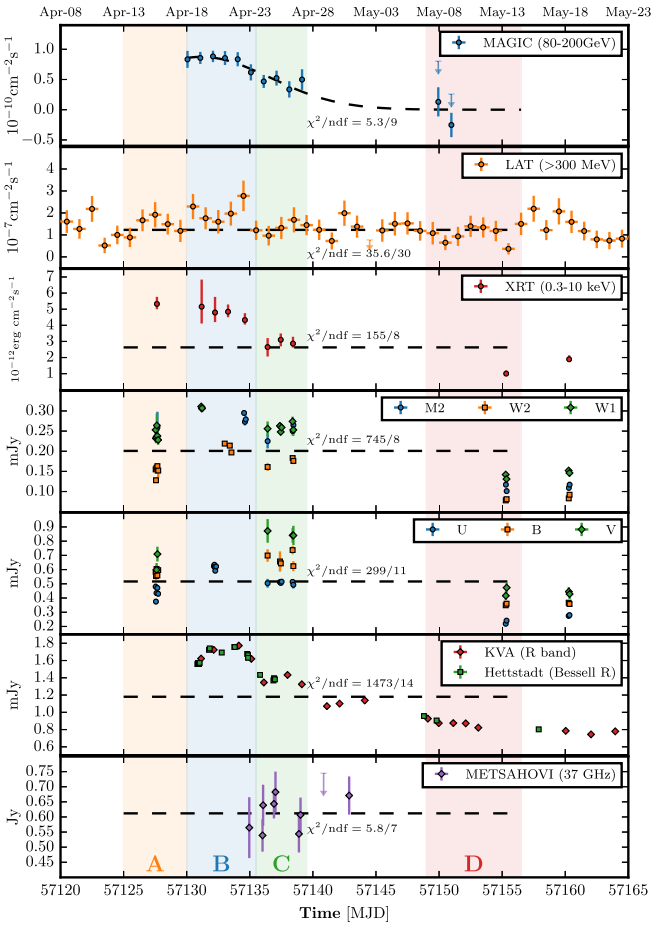

Figure 1. Light curve of PKS 1441+25 at different wavelengths. The shaded areas marked as A, B, C, D depict the different states of the source considered in Section 3.2. Only filters "UVOT-M2," "UVOT-B," and "KVA-R" are used in the fit in the optical–UV bands.

2.6. Near-infrared Observations

NIR observations in the J, H, and K_S bands started on MJD 57141 with CANICA,[88] a direct camera at the 2.1 m telescope of the Guillermo Haro Observatory located at Cananea, Mexico. The flux is estimated by means of differential photometry using the 2MASS catalog (Skrutskie et al. 2006).

2.7. Radio Observations

The observations of PKS 1441+25 with the Metsähovi 13.7 m radio telescope started on MJD 57135. The measurements were made with a 1 GHz-band dual beam receiver centered at 37 GHz. A detailed description of the observation and analysis methods can be found in Teräsranta et al. (1998).

3. RESULTS

3.1. Multi-wavelength Flux Evolution

The MWL light curve is presented in Figure 1. In the VHE band, the no-variability hypothesis can be discarded as it results in a $\chi^2/ndf = 52.5/11$ ($P_{\mathrm{const}}^{B-D} = 2.2 \times 10^{-7}$) for $B + C + D$. A constant fit is also unlikely for the flare in April (B+C) with a $\chi^2/ndf = 26.0/9$ ($P_{\mathrm{const}}^{B+C} = 2.1 \times 10^{-3}$). We gauge the

[88] http://www.inaoep.mx/~astrofi/cananea/canica/

Table 1
Input Parameters for the Emission Models Shown in Figure 2

Period	MJD	$\gamma_{\rm min}$	$\gamma_{\rm b}\,(10^4)$	$\gamma_{\rm max}\,(10^6)$	n_2	B (G)	K (10^3 cm^{-3})	$\nu_{\rm IC}$ [Hz]	CD
A	57125.0–57130.0	80	1.0	1.0	3.55	0.15	2.80	24.2	24
B	57130.0–57135.5	80	1.0	1.0	3.70	0.15	4.00	24.1	25
C	57135.5–57139.5	50	0.8	1.0	3.75	0.17	3.35	24.0	21
D	57149.0–57156.0	50	0.5	0.2	3.90	0.23	2.00	23.6	13
Archival	…	20	10^{-2}	3×10^{-2}	3.05	0.35	70	22.4	7

Note. The other parameters are kept fixed (see the text). The IC peak frequency (in logarithmic scale) and the Compton Dominance (CD) are also reported.

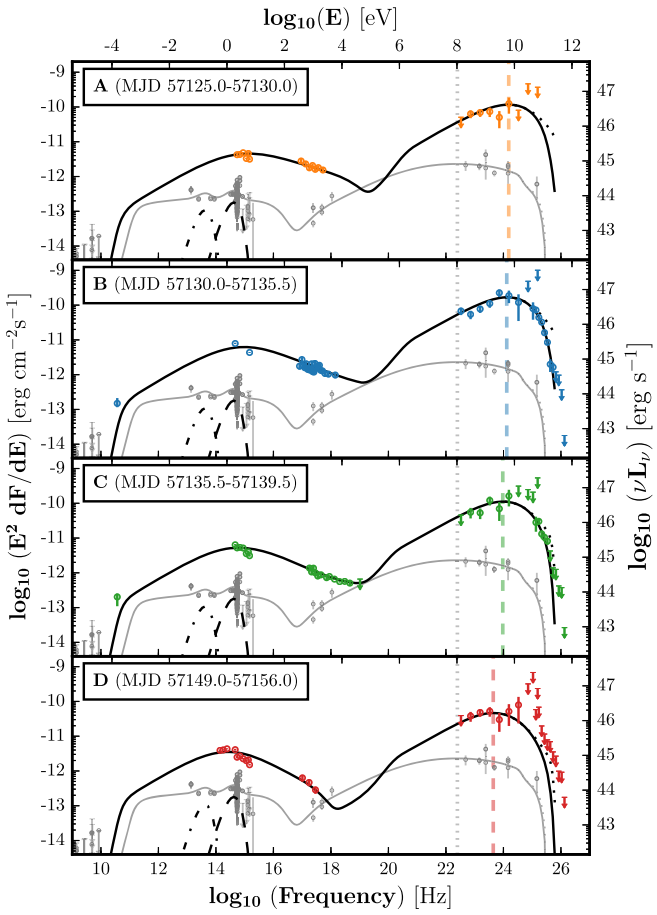

Figure 2. MWL SEDs for PKS 1441+25 for the four states of the source indicated in Figure 1. The broadband emission model for the observed (solid line) and EBL-de-absorbed (dotted line) spectrum, using the model of Domínguez et al. (2011), together with the disk (dashed) and torus (dashed–dotted) emission component are shown. Archival data extracted from ASDC (http://tools.asdc.asi.it) are shown in gray. The VHE spectral points are not corrected for EBL absorption. Vertical lines indicate the IC peaks.

characteristic variability timescale by heuristically fitting the VHE light curve with a Gaussian function. The fit provides a standard deviation $\sigma = 5.5 \pm 1.6$ days (halving flux time of 6.4 ± 1.9 days) and a peak flux of $(8.8 \pm 0.6) \times 10^{-11}$ cm^{-2} s^{-1} ($\chi^2/ndf = 5.3/9$, $P^{B-D}_{\rm Gaussian} = 0.80$). For X-rays, a halving flux time of 7.6 ± 1.7 days was found.

The average flux in B is larger than in C by a factor of $F_B/F_C = 1.80 \pm 0.27$ in VHE. A similar pattern was found in X-rays ($F_B/F_C = 1.58 \pm 0.17$), optical ($F_B/F_C = 1.23 \pm 0.02$) and a hint in the HE (1.40 ± 0.29). No intra-night variability is detected.

3.2. Broadband Spectral Energy Distribution

The MWL spectral energy distributions (SEDs) shown in Figure 2 indicate a shift of both synchrotron and inverse-Compton (IC) peaks to higher energies during the 2015 observation campaign with respect to the archival data, accompanied by a significant variation of the X-ray and HE γ-ray spectral indices. This behavior resembles the less extreme outburst seen in PMN J2345–1555 (Ghisellini et al. 2013), and can be explained by a change in the emitting region location: within the broad-line region (BLR) in the quiescent state to beyond the BLR during the outburst, where the external photon field is dominated by the optical–UV from the BLR or the IR thermal emission of a dusty torus, respectively (conventional framework for γ-loud FSRQ; e.g., Ghisellini & Tavecchio 2009; Tavecchio et al. 2011).

The consequences of this scenario are two-fold: (1) since the radiation energy density of the IR component is much lower than the one associated with the optical–UV photons from the BLR, the electron radiative cooling is less effective and the energy reachable by the acceleration process could be higher, accounting for the shift of the SED peak toward higher energies; (2) given the much lower energy of the external photons, absorption of γ-rays by pair production occurs only above several hundreds of GeV (e.g., Protheroe & Biermann 1997), enabling the detection of FSRQs at VHE. For an emission region well within the BLR, strong absorption features are expected for energies above tens of GeV (see e.g., Liu & Bai 2006; Donea & Protheroe 2003), which are not observed in the 2015 MWL SEDs.

According to this framework, the proposed SED model for the 2015 observations assumes that the emission region is located at a distance $d > R_{\rm BLR}$ from the central compact object. Adopting the simple scaling proposed by Ghisellini & Tavecchio (2009), $R_{\rm BLR}$ depends only on the disk luminosity, $R_{\rm BLR} = 10^{17}(L_{\rm disk}/10^{45})^{1/2}$ cm. The latter can be inferred from the luminosity of the optical broad lines, $L_{\rm disk} \simeq 2.0 \times 10^{45}$ erg s^{-1} (Ghisellini & Tavecchio 2015), resulting in $R_{\rm BLR} = 1.4 \times 10^{17}$ cm. In the same way, the size of the dusty torus can be inferred from a similar scaling law, $R_{\rm IR} = 3.5 \times 10^{18}$ cm. The resulting emission is calculated using the code described in Maraschi & Tavecchio (2003). The emission region is assumed to be spherical (in the source frame) with radius R, in motion with bulk Lorentz factor Γ at angle $\theta_{\rm v}$ with respect to the line of sight. It contains a tangled magnetic field with intensity B and a population of relativistic leptons described by a smoothed broken PWL energy distribution between Lorentz factors $\gamma_{\rm min}$ and $\gamma_{\rm max}$, with a break at γ_b, slopes n_1 and n_2 and normalization K estimated at $\gamma = 1$. The external photon field (dominated by the IR torus emission) is assumed to follow a blackbody spectrum with

Table 2
Upper Limits at 95% Confidence Level on the Relative EBL Opacity α

EBL model	Shape	$\alpha_{\rm best}^{\rm nominal}$	$\alpha_{w/\rm syst}^{UL}$	Param. (best fit)				p-value
				p_0	p_1	p_2	p_3	
PWL	No EBL	...	...	−11.9	−4.6			<0.01
PWL	F08	$1.09^{+0.36}_{-0.31}$	1.72	−11.6	−3.1	...	...	0.50
PWL	D11	$1.09^{+0.37}_{-0.32}$	1.73	−11.5	−3.1	...	...	0.47
PWL	G12	$0.99^{+0.33}_{-0.28}$	1.55	−11.4	−2.7	...	...	0.51
PWL	S14 (max)	$1.09^{+0.37}_{-0.32}$	1.73	−11.5	−3.1	...	...	0.47
PWL	S14 (min)	$2.20^{+0.70}_{-0.61}$	3.41	−11.4	−2.7	...	...	0.54
LP	No EBL	...	...	−11.9	−4.7	3.2	...	0.39
LP	F08	$0.35^{+1.06}_{-1.58}$	1.69	−11.8	−4.2	2.2	...	0.40
LP	D11	$0.18^{+1.20}_{-1.42}$	1.68	−11.8	−4.4	2.7	...	0.39
LP	G12	$0.37^{+0.92}_{-1.63}$	1.53	−11.7	−3.9	2.0	...	0.40
LP	S14 (max)	$0.18^{+1.20}_{-1.42}$	1.68	−11.8	−4.4	2.7	...	0.39
LP	S14 (min)	$1.64^{+1.25}_{-3.56}$	3.40	−11.5	−3.2	0.83	...	0.42
PWLsc	No EBL	...	...	−6.2	1.4	−0.41	0.48	0.27
PWLsc	F08	$0.22^{+1.20}_{-3.21}$	1.70	−7.4	0.46	−0.13	0.47	0.27
PWLsc	D11	$0.15^{+1.23}_{-3.14}$	1.68	−2.7	2.7	−1.9	0.34	0.27
PWLsc	G12	$0.37^{+0.92}_{-3.36}$	1.54	−1.4	2.6	−3.0	0.27	0.27
PWLsc	S14 (max)	$0.15^{+1.23}_{-3.14}$	1.68	−2.7	2.7	−1.9	0.34	0.27
PWLsc	S14 (min)	$1.75^{+1.15}_{-4.74}$	3.40	−2.4	0.39	−5.8	0.17	0.29

Note. The normalization factor 10^{p_0} is given in units of erg cm^{-2} s^{-1}.
References. F08: Franceschini et al. (2008), D11: Domínguez et al. (2011), G12: Gilmore et al. (2012), S14: Scully et al. (2014).

luminosity $L_{\rm IR} = \xi L_{\rm disk}$ ($\xi = 0.6$; following Ghisellini & Tavecchio 2009) and temperature T, diluted within a region of radius $R_{\rm IR}$.

The model also includes γ-ray absorption within the IR radiation field of the torus. Assuming a temperature $T \approx 10^3$ K for the IR torus, the maximum absorption is reached at $E = (m_{\rm e}c^2)^2/2.8\,kT \simeq 1$ TeV in the source frame, with an optical depth $\tau_{\gamma\gamma} \approx (\sigma_{\rm T}/5)(U_{\rm IR}/h\nu_{\rm IR})R_{\rm IR} \approx 250$. Given the large optical depth and the relatively broad spectrum of the target photons, the absorption is appreciable at few hundreds of GeV, i.e., 5% at 200 GeV and 50% at 300 GeV in the observer frame. Note also that an additional softening of the spectrum can be due to the fact that the emission in the VHE band is produced by scattering occurring in the Klein–Nishina (KN) regime (e.g., Blumenthal & Gould 1970; Zdziarski & Krolik 1993; Moderski et al. 2005).

To decrease the number of free parameters, we fix the bulk Lorentz and Doppler factor to $\Gamma = 15$ and $\delta = 20$, close to the average obtained for a large sample of γ-loud FSRQ (Ghisellini & Tavecchio 2015). This implies a viewing angle of the jet $\theta_{\rm v} = 2\overset{\circ}{.}7$, and the aperture angle is fixed to $\theta_{\rm j} = 0.1$ rad ($5\overset{\circ}{.}7$).

We assume that the emission region is located beyond but not very far from the BLR, $d = 5 \times 10^{17}$ cm, implying $R = 5 \times 10^{16}$ cm. The low-energy slope n_1 is fixed to the standard value of 2. The remaining parameters are chosen to reproduce the synchrotron and IC components (see Table 1). To account for the different flux states, an evolution in both the electron distribution and the magnetic field is required. For comparison, the archival data (representation of the quiescent state) were modeled considering the emitting region partially within the BLR (standard framework) at $d = 1.4 \times 10^{17}$ cm, so that the $\gamma\gamma$ optical depth is small as indicated by the highest energy point of the 3FGL spectrum. The ratio between the peak luminosities (Compton Dominance, CD), are reported in Table 1. During the outburst, $\nu_{\rm syn}$ lies more than an order of magnitude outside the FSRQ parameter space in the CD sequence proposed by Finke (2013), indicating a shift in the sequence during flares. The high degree of optical polarization suggests that the emission may come from a compressed region in the jet like an internal shock, which is also an ideal site for electron acceleration/injection.

4. EXTRAGALACTIC BACKGROUND LIGHT CONSTRAINTS

VHE γ-rays from distant blazars can interact with the optical–UV photons from the EBL via pair production (Gould & Schreder 1967; Stecker et al. 1992), resulting in an attenuation of the intrinsic VHE spectrum. The EBL imprint in the γ-ray spectra from distant blazars can be used to constrain the EBL density.

Measurements of the EBL absorption can be derived under some assumptions on the intrinsic spectrum of the source (see, e.g., Ackermann et al. 2012; Abramowski et al. 2013). With a redshift of $z = 0.940$ and a strong detection in the VHE band, PKS 1441+25 allows us to probe EBL models at a distance never explored before in this energy regime with ground-based gamma-ray instruments. However, KN effects together with an expected intrinsic γ-ray absorption in the VHE band (see Section 3.2), can mimic the effect of EBL absorption, making it difficult to disentangle the two effects.

A LRT was used to compare a null hypothesis (no EBL absorption) with respect to the hypothesis of EBL absorption with a scaled opacity $\alpha\,\tau(z, E)$ as in Abdo et al. (2010b). Predicted opacities from Domínguez et al. (2011, τ_{D11}), Franceschini et al. (2008, τ_{F08}), Gilmore et al. (2012, τ_{G12}) and Scully et al. (2014, τ_{S14}) are considered, while α is a free scaling parameter. Different intrinsic spectral shapes were assumed: PWL $dF/dE = 10^{p_0}(E/E_0)^{p_1}$, LP $dF/dE = 10^{p_0}(E/E_0)^{p_1 - p_2 \log_{10} E/E_0}$ and PWLsc $dF/dE = 10^{p_0}(E/E_0)^{p_1}$

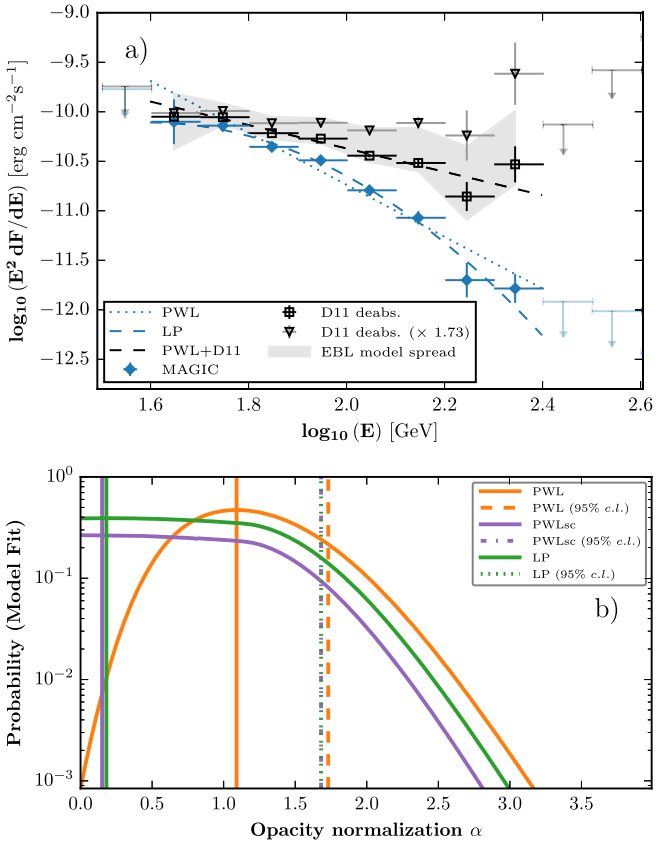

Figure 3. (a) Observed (blue diamonds) and EBL-corrected SED using Domínguez et al. (2011, black squares) for period B. The dotted and dashed lines show the best-fitting PWL, respectively. The gray shaded area accounts for the uncertainties derived by the use of different EBL models (Franceschini et al. 2008; Domínguez et al. 2011; Gilmore et al. 2012). (b) The probability of fit as a function of EBL relative opacity (Domínguez et al. 2011, D11). Only period *B* was considered (without upper limits). The best fit is marked with solid vertical lines and 95% confidence level upper limits with dashed vertical lines.

$\exp[(E/10^{p_2})^{p_3})]$ where E is measured in GeV and $E_0 = 100$ GeV. The limits are reported in Table 2 and an example is given in Figure 3. A possible overall systematic error of $\pm 15\%$ in the absolute energy scale of the instrument is considered. Under the assumption that no curvature is present in the intrinsic VHE spectrum, the measured spectrum is compatible with the present generation of EBL models.

The 95% confidence level limit obtained in this work for Franceschini et al. (2008) is compatible with the one found in Ackermann et al. (2012) for $0.5 \leqslant z \leqslant 1.6$, $\alpha = 1.3 \pm 0.4$, which is obtained from observations with a wide range of redshift values while our UL is calculated for a precise redshift value.

The estimated scaling on the optical depth can be translated into EBL density constraints as shown in Domínguez et al. (2011) and Abramowski et al. (2013). The observed VHE spectrum allow us to constrain the EBL density between 0.21 and 1.13 μm, where the optical depth with respect to the nominal value of Domínguez et al. (2011), $\alpha_{D11} < 1.73$, implies in the local universe $\lambda f_{\lambda=0.5\mu\mathrm{m}} < 8.7$ nW cm^{-2} sr^{-1}.

5. CONCLUSIONS

MAGIC has detected for the first time VHE emission from the $z = 0.940$ blazar PKS 1441+25 during a MWL outburst in 2015 April. PKS 1441+25 is, together with QSO B0218+357, the most distant VHE source detected so far. This allow us to study VHE blazars when the universe was only half of its current age.

The evolution of the MWL SED is studied in the framework of an external Compton emission model. The absence of intrinsic absorption features in the HE and the VHE regime constrains the localization of the emitting region to be just outside of the BLR during this period of high activity, while it is expected to be partially compatible with the BLR during the period of low activity. The SED evolution reveals changes in the electron distribution and the magnetic field.

For the first time, the VHE measurements are used to indirectly probe the EBL at redshifts out to $z \sim 1$ with ground-based gamma-ray instruments. Although an internal cutoff cannot be excluded, the measured VHE spectrum is consistent with a steepening due to attenuation caused by the EBL. Employing state-of-the-art EBL models, upper limits to the EBL density are derived. The upper limits on the opacity calculated under the assumption of an intrinsic spectrum compatible with a PWL function for different EBL models result in $\tau(z, E) < 1.73\ \tau_{D11}$, $\tau(z, E) < 1.72\ \tau_{F08}$, $\tau(z, E) < 1.55\ \tau_{G12}$, $\tau(z, E) < 1.73\ \tau_{S12_{\mathrm{max}}}$ and $\tau(z, E) < 3.41\ \tau_{S12_{\mathrm{min}}}$ for EBL models from Domínguez et al. (2011), Franceschini et al. (2008), Gilmore et al. (2012) and maximum and minimum from Scully et al. (2014), respectively.

We would like to thank the Instituto de Astrofísica de Canarias for the excellent working conditions at the Observatorio del Roque de los Muchachos in La Palma. The financial support of the German BMBF and MPG, the Italian INFN and INAF, the Swiss National Fund SNF, the ERDF under the Spanish MINECO (FPA2012-39502) and MECD (FPU13/00618), and the Japanese JSPS, and MEXT is gratefully acknowledged. This work was also supported by the Centro de Excelencia Severo Ochoa SEV-2012-0234, CPAN CSD2007-00042, and MultiDark CSD2009-00064 projects of the Spanish Consolider-Ingenio 2010 programme, by grant 268740 of the Academy of Finland, by the Croatian Science Foundation (HrZZ) Project 09/176 and the University of Rijeka Project 13.12.1.3.02, by the DFG Collaborative Research Centers SFB823/C4 and SFB876/C3, and by the Polish MNiSzW grant 745/N-HESS-MAGIC/2010/0.

The *Fermi*-LAT Collaboration acknowledges support for LAT development, operation and data analysis from NASA and DOE (United States), CEA/Irfu and IN2P3/CNRS (France), ASI and INFN (Italy), MEXT, KEK, and JAXA (Japan), and the K.A. Wallenberg Foundation, the Swedish Research Council and the National Space Board (Sweden). Science analysis support in the operations phase from INAF (Italy) and CNES (France) is also gratefully acknowledged.

We thank the *Swift* team duty scientists and science planners. L.P. acknowledges the PRIN-INAF 2014 financial support.

REFERENCES

Abdo, A. A., Ackermann, M., Ajello, M., et al. 2010a, ApJS, 188, 405
Abdo, A. A., Ackermann, M., Ajello, M., et al. 2010b, ApJ, 723, 1082
Abramowski, A., Acero, F., Aharonian, F., et al. 2013, A&A, 550, A4
Acero, F., Ackermann, M., Ajello, M., et al. 2015, ApJS, 218, 23
Ackermann, M., Ajello, M., Albert, A., et al. 2012, Sci, 338, 1190
Ackermann, M., Ajello, M., Allafort, A., et al. 2013, ApJS, 209, 34
Aleksić, J., Ansoldi, S., Antonelli, L. A., et al. 2015, APh, 72, 76
Atwood, W. B., Abdo, A. A., Ackermann, M., et al. 2009, ApJ, 697, 1071

Blumenthal, G. R., & Gould, R. J. 1970, RvMP, 42, 237
Burrows, D. N., Hill, J. E., Nousek, J. A., et al. 2005, SSRv, 120, 165
Carrasco, L., Miramon, J., Porras, A., et al. 2015, ATel, 6895
Domínguez, A., Primack, J. R., Rosario, D. J., et al. 2011, MNRAS, 410, 2556
Donea, A. C., & Protheroe, R. J. 2003, APh, 18, 377
Finke, J. D. 2013, ApJ, 763, 134
Fomin, V. P., Sepanian, A. A., Lamb, R., et al. 1994, APh, 2, 137
Franceschini, A., Rodighiero, G., & Vaccari, M. 2008, A&A, 487, 837
Gehrels, N., Chincarini, G., Giommi, P., et al. 2004, ApJ, 611, 1005
Ghisellini, G., & Tavecchio, F. 2009, MNRAS, 396, 105
Ghisellini, G., & Tavecchio, F. 2015, MNRAS, 448, 1060
Ghisellini, G., Tavecchio, F., Foschini, L., Bonnoli, G., & Tagliaferri, G. 2013, MNRAS, 432, 66
Gilmore, R. C., Somerville, R. S., Primack, J. R., & Domínguez, A. 2012, MNRAS, 422, 3189
Gould, R. J., & Schreder, G. P. 1967, PhRv, 155, 1404
Harrison, F. A., Craig, W. W., Christensen, F. E., et al. 2013, ApJ, 770, 103
Kalberla, P. M. W., Burton, W. B., & Hartmann, D. 2005, A&A, 440, 775
Liu, H. T., & Bai, J. M. 2006, ApJ, 653, 1089
Maraschi, L., & Tavecchio, F. 2003, ApJ, 593, 667
Mirzoyan, R. & (on behalf of the MAGIC Collaboration) 2015, ATel, 7416
Moderski, R., Sikora, M., Coppi, P. S., & Aharonian, F. 2005, MNRAS, 363, 954–66
Mukherjee, R. (on behalf of the VERITAS Collaboration) 2015, ATel, 7433
Nolan, P. L., Abdo, A. A., Ackermann, M., et al. 2012, ApJS, 199, 31
Ojha, R. (on behalf of the Fermi-LAT Collaboration) 2015, ATel, 6878
Pacciani, L. 2015, ATel, 7402
Perri, M., Puccetti, S., Spagnuolo, N., et al. 2014, The NuSTAR Data Analysis Software Guide, http://heasarc.gsfc.nasa.gov/docs/nustar/analysis/nustar_swguide.pdf
Protheroe, R. J., & Biermann, P. L. 1997, APh, 6, 293
Pursimo, T., & Ojha, R. 2015, ATel, 6923
Roming, P. W. A., Kennedy, T. E., Mason, K. O., et al. 2005, SSRv, 120, 95
Schlafly, E. F., & Finkbeiner, D. P. 2011, ApJ, 737, 103
Schultz, G. V., & Wiemer, W. 1975, A&A, 43, 133
Scully, S. T., Malkan, M. A., & Stecker, F. W. 2014, ApJ, 784, 138
Shaw, M. S., Romani, R. W., Cotter, G., et al. 2012, ApJ, 748, 49
Sitarek, J., Becerra-González, J., Dominis Prester, D., et al. 2015, in PoS ICRC 2015, 825, Proc. 34th ICRC (The Hague, The Netherlands)
Skrutskie, M. F., Cutri, R. M., Stiening, R., et al. 2006, AJ, 131, 1163
Smith, P. S., & Tutar Ozdarcan, D. 2015, ATel, 7417
Stecker, F. W., DeJager, O. C., & Salamon, M. H. 1992, ApJL, 390, L49
Tavecchio, F., Becerra Gonzalez, J., Ghisellini, G., et al. 2011, A&A, 534, A86
Teräsranta, H., Tornikoski, M., Mujunen, A., et al. 1998, A&AS, 132, 305
Zanin, R., Carmona, E., Sitarek, J., et al. 2013, in Proc. 33th ICRC (Rio de Janeiro, Brazil), http://www.cbpf.br/~icrc2013/papers/icrc2013-0773.pdf
Zdziarski, A. A., & Krolik, J. H. 1993, ApJL, 409, L33